PARAMETER ESTIMATION AND UNCERTAINTY QUANTIFICATION OF GEOTHERMAL RESERVOIR MODELS USING THE ADAPTIVE DELAYED ACCEPTANCE METROPOLIS-HASTINGS ALGORITHM

Tiangang Cui[1], Colin Fox[2], Mike O'Sullivan[1]
[1]Department of Engineering Science, The University of Auckland
[2]Deparment of Physics, Unversity of Otago
tcui001@aucklanduni.ac.nz, fox@physics.otago.ac.nz, m.osullivan@auckland.ac.nz

Keywords: *model calibration, inverse problem, Bayesian inference, Markov chain Monte Carlo*

ABSTRACT

We present two applications of the adaptive delayed acceptance Metropolis-Hastings algorithm (ADAMH) for the automated calibration of large-scale geothermal reservoir models, within the framework of Bayesian inference. ADAMH is a two step Markov chain Monte Carlo (MCMC) algorithm that the uses adaptivity and coarse scale models to enhance the sampling performance. The first study case is a 1D well discharge test model with synthetic data, and the second case demonstrates an application on a 3D natural state model with measured data. The latter consists of 10,000 model parameters and each model simulation takes more than 30 minutes. Compare to the standard MCMC algorithms, ADAMH provides significant improvements in the sampling efficiency.

1 INTRODUCTION

In setting up numerical models of geothermal reservoirs, the estimation of spatially distributed parameters and the quantification of the associated uncertainties are important topics for investigation. Because the parameters of interest such as porosity and permeability are usually spatially distributed, highly heterogeneous and anisotropic, and data are usually sparse, conditioning the parameters on data is an ill-posed inverse problem (Hadamard, 1902; Jaynes, 1984). This means that there exist a range of feasible parameters that are consistent with the measured data, and hence a range of possible model predictions. Thus, the assessment of parameters and model predictions require summarizing information over this range of feasible parameters.

This problem can be naturally fitted into the Bayesian inferential framework by constructing the posterior distribution over model parameters conditioned on measured data (Kaipio and Somersalo, 2004). The posterior distribution quantifies the relative probability of a set of parameters being correct, and hence robust model predictions and uncertainty quantification can be calculated as expectations of desired quantities over the posterior distribution. Because of the high dimensionality of the parameter space and nonlinearity of the posterior distribution for geothermal problems, the most efficient way for computing expectations of summary statistics is by Monte Carlo integration, using samples distributed according to the posterior distribution. The best technology currently for drawing such samples is MCMC sampling. The role of Bayesian inference in geothermal model calibration and preliminary studies on this topic can be found in Cui (2005); Cui et al. (2006).

Traditionally, this approach has been considered to be computationally prohibitive for large scale problems such as geothermal reservoir models. However, the adaptive delayed acceptance Metropolis-Hastings algorithm (ADAMH) developed by *Cui et al.* (2011) allows us to apply MCMC techniques to the title problem at a scale that has previously been infeasible. ADAMH enhances the computational efficiency of the Metropolis-Hastings algorithm (MH) (Metropolis et al., 1953; Hastings, 1970) by employing a coarse scale model and state-of-the-art techniques in adaptive MCMC sampling (Haario et al., 2001; Roberts and Rosenthal, 2007).

We first validate ADAMH on a 1D homogeneous geothermal reservoir model with synthetic data. This model consists of 7 parameters, and each model simulation costs about 2.60 seconds CPU time. ADAMH shows a speed-up factor about 4.1 compare to the standard MH. Then, ADAMH is applied to the estimation of the heterogeneous and anisotropic permeability distribution and the heterogeneous boundary conditions of a 3D natural state model of a two phase geothermal reservoir. There are about 10^4 parameters in the natural state model, and each model simulation requires about 30 to 50 minutes of CPU time, which makes it virtually impossible for the standard MH algorithm to be applied. ADAMH achieves a speed-up factor about 7.7 compare to the standard MH. We are able to run 11,200 iterations in about 40 days. The sampling results show good agreement between the estimated temperature profiles and the measured data.

The TOUGH2 computer package (Pruess, 1991) is used to simulate the geothermal reservoir models presented in this study. For compactness, the governing equations and numerical methods are not discussed here, and we refer the readers to Pruess (1991).

This paper is organized as follows: Section 2 gives discussions of the Bayesian inferential framework for inverse problems. Section 3 discusses the efficiency of MCMC sampling, and presents the details of ADAMH. In Section 4, we present a case study on an 1D well discharge test model with synthetic data. In Section 5, we present a study on 3D geothermal reservoir model with measured data. Section 6 offers some conclusions and discussion.

2 BAYESIAN FORMULATION

In a Bayesian framework, the unknown parameters $\mathbf{x}$ are considered as random variables, and a posterior distribution $\pi(\mathbf{x} \mid \mathbf{d})$ over parameters $\mathbf{x}$ conditioned on measurements $\mathbf{d}$ can be constructed using the probabilistic model for various uncertainties associated with the inverse problem. The commonly used stochastic relationship is

$$\mathbf{d} = F(\mathbf{x}) + \mathbf{e}, \tag{1}$$

where $F : \mathbf{x} \rightarrow \mathbf{d}$ is a deterministic TOUGH2 model simulation, and $\mathbf{e}$ is a noise vector that represents all the uncertainties associated with the map from parameters to data, such as measurement noise and modelling error. Following Bayes' theorem, the unnormalized posterior distribution

$$\pi(\mathbf{x} \mid \mathbf{d}) \propto \pi(\mathbf{d} \mid \mathbf{x})\pi(\mathbf{x}) \tag{2}$$

is given as a product of the likelihood function $\pi(\mathbf{d} \mid \mathbf{x})$ and prior distribution $\pi(\mathbf{x})$. From (1) and the Gaussian assumption about the noise $\mathbf{e}$ (Higdon et al., 2003), we can deduce that the likelihood function has the form

$$\pi(\mathbf{d} \mid \mathbf{x}) \propto \exp\left(-\frac{1}{2\sigma_e^2}\|\mathbf{d} - F(\mathbf{x})\|^2\right), \tag{3}$$

where $\|\cdot\|$ is the Euclidean norm.

The prior distribution $\pi(\mathbf{x})$ quantifies the relative probability for a given set of parameters $\mathbf{x}$ in the absence of field measurements (Jaynes, 1968). Formulating the prior distribution for a subsurface modeling problem usually consists of: (i) Choosing an appropriate representation of the unknown parameters. As discussed in Hurn et al. (2003), this is a composite part of prior modeling since expressing certain types of knowledge is simpler in some representations than others, and solutions that cannot be represented are excluded. (ii) Deriving the spatial statistics for the chosen parametrization by expert knowledge of allowable parameter values, previous measurements, modeling of processes that produce the unknowns, or a combination of these.

3 MCMC SAMPLING

3.1 Standard Metropolis Hastings

To effectively solve the inverse problem, the posterior distribution (2) is sampled by the Markov Chain Monte Carlo (MCMC) method, and hence summary statistics can be estimated from samples. MCMC algorithms draw samples from the posterior distribution by generating a sequence, or "chain", of solutions that have the ergodic property, i.e, that allow expectations over the posterior distribution to be replaced by averages over the chain. Informally, we think of an ergodic chain as one that spends time in each region of parameter space proportional to the posterior probability of that region. Almost all implementations of MCMC sampling employ Metropois-Hastings dynamics (MH) (Metropolis et al., 1953; Hastings, 1970). At step n, given state $\mathbf{x}_n = \mathbf{x}$, one step of MH can be written as follows:

1. Generate a candidate state $\mathbf{y}$ by the proposal distribution $\mathbf{y} = q(\mathbf{x}, \cdot)$.
2. With probability

$$\alpha(\mathbf{x}, \mathbf{y}) = 1 \wedge \frac{\pi(\mathbf{y}|\mathbf{d})}{\pi(\mathbf{x}|\mathbf{d})}\frac{q(\mathbf{y}, \mathbf{x})}{q(\mathbf{x}, \mathbf{y})}, \tag{4}$$

set $\mathbf{x}_{n+1} = \mathbf{y}$, otherwise $\mathbf{x}_{n+1} = \mathbf{x}$.

The symbol $\wedge$ denotes the minimum of two factors.

MH generates a highly correlated random sequence of parameters (or solutions), $\mathbf{x}_1, \mathbf{x}_2, \ldots, \mathbf{x}_N$ having the Markov property, with a limiting distribution equal to the desired posterior distribution, i.e., $\mathbf{x}_i \sim \pi(\mathbf{x} \mid \mathbf{d})$ for large i. Hence $\mathbf{x}_i$ and $\mathbf{x}_{i+1}$ will be very similar, however for large lags, i.e. $j \gg i$, the parameter $\mathbf{x}_i$ and $\mathbf{x}_j$ may be viewed as independent samples from the posterior distribution. Because our goal is to estimate the expectation values of statistics of interest, the performance of MCMC sampling is characterized by the number of statistically independent samples that can be drawn. The *statistical efficiency* of MH is quantified by the number of iterations required to generate a statistically independent sample, which is calculated by estimating the integrated autocorrelation time of some statistics of interest over the chain (Goodman and Sokal, 1989).

Tuning the variables that control the scale and orientation of the proposal distribution is crucial for achieving statistical efficiency. One motivated example is the commonly used multivariate Gaussian proposal, i.e., $\mathbf{y} \sim N(\mathbf{x}, \gamma^2\Sigma)$, where Σ is the covariance matrix and γ is the scale variable. Gelman et al. (1996); Roberts et al. (1997); Roberts and Rosenthal (2001) show that for a d-dimensional parameter space, the optimal choice of the scale variable is $\gamma \approx 2.38/\sqrt{d}$ given several theoretical assumptions. They also showed that the acceptance rate of about 0.23 gives the optimal statistical efficiency for a high dimensional target distribution. Traditionally, the modeler has to adjust these scale variables in a "trial and run" manner, which is very time consuming for high dimensional problems. Recent advances in adaptive MCMC sampling such as the adaptive Metropolis algorithm (AM) (Haario et al., 2001) automate the tuning process by using the sampling history.

Apart from designing the proposals, computational difficulty arises in MCMC sampling mainly because MH requires sequential evaluation of the posterior density at each iteration, and many thousands or millions of iterations are necessary to give sufficiently accurate estimates. Hence, we have to consider the *computational efficiency* of MH in practice, i.e., the computing time for generating a statistically independent sample is used instead of the number of iterations. To improve computational efficiency, it not only necessary to design efficient proposals that adequately explore the parameter space, but it also requires the reduction of the computing time per iteration. ADAMH reduces the computing time per iteration by using a computationally fast coarse model.

3.2 ADAMH

Suppose we have a coarse model $F(\cdot)$ that is computationally faster than the accurate model $F(\cdot)$ used in the likelihood (3). By employing the approximation error model of Kaipio and Somersalo (2007), *Cui et al.* (2011) introduced an approximate posterior distribution

$$\pi_n^*(\mathbf{x}|\mathbf{d}) \propto \exp\left\{-\frac{1}{2}\|L[F^*(\mathbf{x}) + \boldsymbol{\mu}_B - \mathbf{d}]^T\|^2\right\}\pi(\mathbf{x}), \tag{5}$$

where $L^T L = (\Sigma_B + \Sigma_\mathbf{e})^{-1}$. In the above formulae, the mean μ_B and covariance Σ_B define a multivariate normal distribution which is used to capture the model

reduction error between the coarse model and accurate model. ADAMH empirically estimates μ_B and Σ_B from the past history of MCMC sampling.

At step n, suppose we have $\mathbf{x}_n = \mathbf{x}$, One step of ADAMH is given as follows:

1. Generate a proposal $\mathbf{y}$ from the adaptive proposal distribution $q_n(\mathbf{x}, \cdot)$.
2. Let
$$\alpha_n(\mathbf{x}, \mathbf{y}) = \min\left[1, \frac{\pi_n^*(\mathbf{y}) q_n(\mathbf{y}, \mathbf{x})}{\pi_n^*(\mathbf{x}) q_n(\mathbf{x}, \mathbf{y})}\right].$$
With probability $\alpha_n(\mathbf{x}, \mathbf{y})$, accept $\mathbf{y}$ to be used as a proposal for the standard MH. Otherwise use $\mathbf{y} = \mathbf{x}$ as a proposal.
3. Let
$$\beta_n(\mathbf{x}, \mathbf{y}) = 1 \wedge \frac{\pi(\mathbf{y} \mid \mathbf{d})}{\pi(\mathbf{x} \mid \mathbf{d})} \frac{\pi_n^*(\mathbf{x} \mid \mathbf{d})}{\pi_n^*(\mathbf{y} \mid \mathbf{d})}.$$
With probability $\beta_n(\mathbf{x}, \mathbf{y})$ accept $\mathbf{y}$ setting $\mathbf{x}_{n+1} = \mathbf{y}$. Otherwise reject $\mathbf{y}$ setting $\mathbf{x}_{n+1} = \mathbf{x}$. Note that the candidate $\mathbf{y} = \mathbf{x}$ has acceptance probability 1.
4. Update the approximation $\pi_n^*(\cdot)$ by updating the mean μ_B and covariance Σ_B.
5. Update the adaptive proposal $q_n(\mathbf{x}, \cdot)$.

In the above algorithm, the adaptive proposal in step 1 and 5 has to be specified by the user. We use the modified block Metropolis update introduced by Cui et al. (2011). In the first step of ADAMH, the approximate posterior distribution is used to reject proposals that are have lower acceptance probability α. If the approximate posterior distribution is close enough to the true posterior, the first step should be able to eliminate most of the "bad" candidates. Then the use of the second step acceptance probability β ensures that the samples are drawn from the correct posterior distribution. For an accurate approximate posterior distribution, the second step acceptance probability must close to 1. Since the computing time of the approximation is lower than the exact posterior distribution, the average computing time per iteration in ADAMH is reduced compare to standard MH, and hence the computational efficiency is improved.

It is worth mentioning that the coarse model usually has a non-negligible discrepancy with the forward model. The approximate posterior (5) uses the enhanced error model of Kaipio and Somersalo (2007) to capture this discrepancy. As shown by *Cui et al.* (2011), this treatment gives a more accurate approximate posterior distribution. Without using the enhanced error model, the approximation solely based on the coarse scale model would lead to a very low seconds step acceptance probability. The original enhanced error model requires a large amount of off-line computing to estimate the approximation from the prior distribution. ADAMH significantly saves computing time by estimating the approximation (5) on-line using adaptivity. This approach also provides a more accurate estimation of the approximation over the posterior distribution. *Cui et al.* (2011) provides a detailed proof of the ergodicity of this algorithm, and analysis on the speed-up factor of ADAMH compared to the standard MH.

4 1D MODEL

We first validate ADAMH by a well discharge test model with synthetic data. Based on assumption that all flows into the well come through a single layer feedzone, An one dimensional radial symmetry forward model with 640 blocks is built to infer the near-well properties of the reservoir, as shown in the plot (a) of Figure 1. A high resolution grid is used immediately outside the wellbore and the thickness increases exponentially outside this region, where the wellbores is located in the centre of the models. The coarse model is build by coarsening the grid of the forward model to a coarse grid with 80 blocks, as shown in the plot (b) of Figure 1. The CPU time of evaluating the forward model and the coarse model are 2.60 and 0.29 seconds on a DELL T3400 workstation.

The parameters of interest are the porosity, permeability, initial conditions and the hyperparameters in the van Genuchten-Mualem relative permeability model, as well as the initial vapor saturation (S_{v0}) and initial pressure (p_0) that are used to represent the initial thermodynamics state of the two-phase system. These make up the seven unknown parameters for the data simulation:

$$\mathbf{x} = (\phi, \log_{10}(k), p_0, S_{\text{v0}}, m, S_{\text{rl}}, S_{\text{ls}}).$$

Note that the permeability k is represented on a base 10 logarithmic scale.

To test ADAMH, a set of synthetic data is generated over 80 days with production rates varying smoothly from about 4 kg/seconds to about 6 kg/seconds. The forward model and the model parameters $\mathbf{x} = (0.12, 1.5 \cdot 10^{-15}, 120, 0.1, 0.65, 0.25, 0.91)$ are employed to generate the synthetic data. The production rate and the noise corrupted pressure and flowing enthalpy response are shown in plots (c)-(e) in Figure 1, where the noise follow an i.i.d. Gaussian distribution with standard deviations $\sigma_{\text{p}} = 3$ bar for pressure and $\sigma_{\text{h}} = 30$ kJ/kg for the flowing enthalpy. This gives

$$\mathbf{\Sigma_e} = \begin{pmatrix} \sigma_{\text{h}}^2 \mathbf{I}_n & 0 \\ 0 & \sigma_{\text{p}}^2 \mathbf{I}_n \end{pmatrix}$$

in the likelihood function (3), and observed data $\mathbf{d} = (\mathbf{d}_{\text{h}}, \mathbf{d}_{\text{p}})^T$ comprises the observed flowing enthalpy and pressure, and n is number of measurements. ADAMH achieves a second step acceptance rate of 97%, and the estimated IACT of the log-likelihood function is 145.87. This gives a speed-up factor about 4.1 compare to the standard MH.

The model predictions and the 95% credible intervals over an 80-day period are shown in Figure 2, with pressure on the left and enthalpy on the right. For both predictions, the means follow the observed data reasonably well. The histograms of the marginal distributions of the parameter $\mathbf{x}$ (see first two rows of Figure 3) show skewness in porosity and two of the hyperpa-

rameters of the van Genuchten-Mualem relative permeability model (m and S_{rl}). The scatter plots between parameters show strong negative correlations between the permeability (on base 10 logarithmic scale) and the initial pressure, see the first plot of last row of Figure 3. There also exists strong negative correlations between the initial saturation and one of the hyperparameters of the van Genuchten-Mualem (S_{ls}), see the second plot of last row of Figure 3.

5 3D MODEL

Next we apply ADAMH to a 3D natural state modelling problem. We aim to estimate the large scale permeability structure and boundary conditions from steady state temperature distributions. The temperature measurements are presented in Figure 6, manual calibration results and trial runs of MCMC sampling suggest that the model mis-fit has standard deviation $\sigma_T = 7.5\,^{\circ}\text{C}$. Thus, $\mathbf{\Sigma_e} = \sigma_{\text{T}}^2\mathbf{I}_n$ is used in the likelihood function (3), where n is the number of observations.

The geological setting of the geothermal reservoir model we demonstrate here is summarized in Cui et al. (2011). The model covers a volume of 12.0 km by 14.4 km extending down to 3050 meters below the sea level. Relatively large blocks were used in the outside of the model and then they were progressively refined near the wells to achieve a well-by-well allocation to the blocks. The 3D structure of the forward model has $26,005$ blocks, which is shown in plot (a) of Figure 4, where the blue lines in the middle of the grid are wells drilled into the reservoir. To speed up the computation, a coarse model with $3,335$ blocks is constructed by combining adjacent blocks in the x, y and z directions of the forward model (see plot (b) of Figure 4). A coarser level of grid resolution is not used here because further coarsening of the grid structure would produce a model that cannot reproduce the convective plume in the reservoir. Each simulation of the forward model takes about 30 to 50 minutes CPU time on a DELL T3400 workstation, and the computing time for the coarse model is about 1 to 1.5 minutes (roughly 3% of the forward model). The computing time for these models is sensitive to the input parameters.

The permeabilities are represented by a pixel based representation with the same resolution as the coarse model. A first order Gaussian Markov random field (GMRF) model (Rue and Held, 2005) is used to formulate the prior distribution for each of the x, y, and z direction of permeabilities. Thus, we have $10,005$ unknown permeabilities $\left\{\mathbf{k}^{(x)}, \mathbf{k}^{(y)}, \mathbf{k}^{(z)}\right\}$.

The top of the model is assumed to be "open", which allows the model to have direct connection with the atmosphere. Atmosphere pressure and temperature are used as the boundary conditions at the top of the model. The model covers a sufficiently large area so that the flows through the side of the boundary are negligible in the natural state modelling, and hence the sides of the model are treated as no-flow boundaries. At the base of the model, a distribution of very hot water is injected to represent the upflow from depth, which also has to be estimated. We parametrize this mass input by a radial basis function (RBF) with the Gaussian kernel function. The RBF representation uses an unknown 41-dimensional weighting vector $\mathbf{w}$ to control the shape of the distribution.

For compactness, we refer to Cui et al. (2011) for the detailed derivation of the representation of unknowns. Overall, we have the parameters

$$\mathbf{x} = \left\{\mathbf{k}^{(x)}, \mathbf{k}^{(y)}, \mathbf{k}^{(z)}, \mathbf{w}\right\}$$

to be estimated. We are able to sample the posterior distribution by ADAMH for about $11,200$ iterations in 40 days. ADAMH achieves about 10% acceptance rate in the first step, and 74% acceptance rate in the second step. The estimated speed-up factor is about 7.7 compared to the sandard MH algorithm.

The mean and standard deviation of the temperature profiles are estimated as sample averages over model realizations. We compare these estimations with the measured data in Figure 6. The solid black lines are the estimated mean temperatures, dashed black lines are the 95% percent credible interval, and measured data are shown as red crosses. The green and gray lines represent outputs of the foaward model and the coarse model for various realizations, respectively.

The temperature distributions are shown in Figure 7, where (a) shows the mean temperature distribution, the standard deviation of the temperature distribution is shown in (b), and the temperature distributions of the two realizations from the Markov chain (one from the middle and another from the end) are presented in (c) and (d). From these plots, we can observe that there is one hot plume in the model, and the top and the bottom of this hot plume have larger variations in temperature than the rest of the model.

The mean distribution of the mass input shows that most of the injected hot water occurs at the bottom of the inner resistivity boundary. This corresponds to the opinion of geologists that the major source of deep hot water occurs at the intersection of two geological faults in this area. The standard deviation and two realizations of this distribution suggest that the variation among the samples is very small.

The reasonably large variations in the reconstructed permeability distributions suggest that there exists ambiguities in the permeability distributions, and this may be caused by the sparsely measured data. This effect is more significant in the region close to the boundary of the reservoir, where no measured data are available. We can either give more accurate quantifications to these ambiguities by running the chain for a very long time, or remove these ambiguities by imposing a stronger prior distribution or using different parameterizations of the permeability distributions.

6 DISCUSSION

We applied the adaptive delayed acceptance Metropolis-Hastings algorithm (ADAMH) to the calibration of two geothermal reservoir models. ADAMH demonstrates efficiency in both study cases. In the calibration of the 3D geothermal reservoir model, ADAMH offers a significant improvement compared to the standard MH algorithm, which is a task that

was not possible with existing MCMC methods. By using adaptive approximations and adaptive proposal distributions, ADAMH is a fully automated algorithm and can be implemented for other problems without modifying the existing code.

The approximate posterior distribution we used here is based on the coarse scale models. However, other methods of model order reduction could also be fitted into ADAMH, such as the stochastic Galerkin (Marzouk and Najm, 2009) and proper orthogonal decomposition (Willcox and Peraire, 2002). These methods potentially could offer a more accurate and computationally faster approximate posterior distribution. It is also important that investigating strategies for designing proposal distributions that traverse the parameter space more efficiently.

REFERENCES

Cui, T. (2005). Bayesian inference for geothermal model calibration. Master's thesis, The University of Auckland, Auckland, New Zealand.

Cui, T., C. Fox, G. Nicholls, and M. J. O'Sullivan (2006). Bayesian inference for geothermal model calibration. *Preceedings of the 28th New Zealand Geothermal Workshop*, Auckland, New Zealand

Cui, T., C. Fox, and M. J. O'Sullivan (2011), Adaptive error modelling in MCMC sampling for large scale inverse problem, *Tech. Rep. no. 686*, University of Auckland, Faculty of Engineering.

Cui, T., C. Fox, and M. J. O'Sullivan (2011). Bayesian calibration of a large scale geothermal reservoir model by a new adaptive delayed acceptance metropolis hastings algorithm. *Water Resource Research*, accepted for publication.

Gelman, A., G. O. Roberts, and W. R. Gilks (1996). Efficient Metropolis jumping rules. In J. O. Berger, J. M. Bernardo, A. P. Dawid, D. V. Lindley, and A. F. M. Smith (Eds.), *Bayesian Statistics*, Volume 5, Oxford, pp. 599–608. Oxford University Press.

Goodman, J. and A. Sokal (1989). Multigrid Monte Carlo method: Conceptual foundations. *Physical Review D 40(6)*, 2035–2071.

Haario, H., E. Saksman, and J. Tamminen (2001). An adaptive Metropolis algorithm. *Bernoulli 7*, 223–242.

Hadamard, J. (1902). Sur les problemes aux derivees partielles et leur signification physique. [on the problems about partial derivatives and their physical significance]. *Princeton University Bulletin 13*, 49–52.

Hastings, W. (1970). Monte Carlo sampling using Markov chains and their applications. *Biometrika 57*, 97–109.

Higdon, D., H. Lee, and C. Holloman (2003). Markov chain Monte Carlo-based approaches for inference in computationally intensive inverse problems. In J. M. Bernardo, M. J. Bayarri, J. O. Berger, A. P. Dawid, D. Heckerman, A. F. M. Smith, and M. West (Eds.), *Bayesian Statistics 7*, pp. 181–197. Oxford University Press.

Hurn, M. A., O. Husby, and H. Rue (2003). Advances in Bayesian image analysis. In P. J. Green, N. L. Hjort, and S. Richardson (Eds.), *Highly Structured Stochastic Systems*, pp. 301–322. Oxford University Press.

Jaynes, E. T. (1968). Prior probability. *IEEE Transactions on System Science and Cybernetics sec-4 (3)*, 227–241.

Jaynes, E. T. (1984). Prior information and ambiguity in inverse problems. In D. W. McLaughlin (Ed.), *Inverse Problems*, Volume 14 of *SIAM-AMS Proceedings*.

Kaipio, J. and E. Somersalo (2004). *Statistical and Computational Inverse Problems*. Springer-Verlag.

Kaipio, J. P. and E. Somersalo (2007). Statistical inverse problems: Discretization, model reduction and inverse crimes. *Journal of Computational and Applied Mathematics 198(2)*, 493–504.

Marzouk, Y. M., Najm, H. N. (2009). Dimensionality reduction and polynomial chaos acceleration of Bayesian inference in inverse problems. *Journal of Computational Physics* , *228*, 1862–1902.

Metropolis, N., A. W. Rosenbluth, M. N. Rosenbluth, A. H. Teller, and E. Teller (1953). Equation of state calculations by fast computing machines. *Journal of chemical physics 21*, 1087–1092.

Pruess, K. (1991). *TOUGH2 - A General-Purpose Numerical Simulator for Multiphase Fluid and Heat Flow*. Berkeley, California: Lawrence Berkeley National Laboratory.

Roberts, G. O., A. Gelman, and W. R. Gilks (1997). Weak convergence and optimal scaling of random walk Metropolis algorithms. *Annals of Applied Probability 7*, 110–120.

Roberts, G. O. and J. S. Rosenthal (2001). Optimal scaling for various Metropolis-Hastings algorithms. *Statistical Science 16*, 351–367.

Roberts, G. O. and J. S. Rosenthal (2007). Coupling and ergodicity of adaptive MCMC. *Journal of Applied Probability 44*, 458–475.

Rue, H. and L. Held (2005). *Gaussian Markov Random Fields: Theory and Applications*. Chapman & Hall.

Willcox, K. and Peraire J. (2002). Balanced Model Reduction via the Proper Orthogonal Decomposition. *AIAA Journal*, *40(11)*, 2323–30.

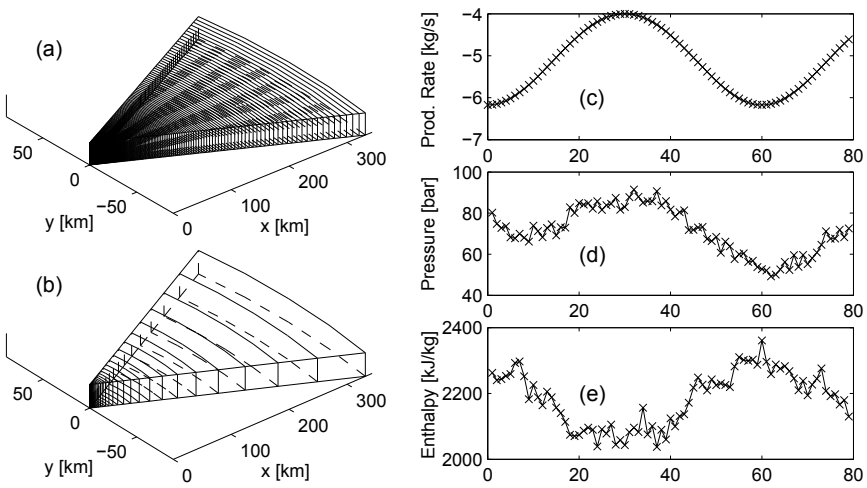

Figure 1: Finite volume grids used for well discharge test analysis and data sets used for well discharge test. (a): the forward model (640 blocks), (b): the coarse model (80 blocks), (c): the production rate (kg/seconds), (d): the pressure (bar), and (e): the flowing enthalpy (kJ/kg).

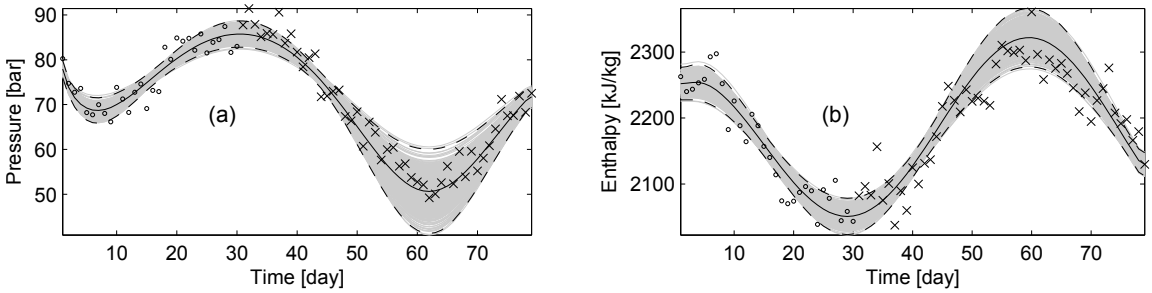

Figure 2: Predictions for the synthesis data set. (a): pressure, (b): flowing enthalpy. The circles and the crosses are the training data and validation data, respectively; the solid line and dashed lines are the mean prediction and 95% credible interval, respectively; and the shaded lines represent the predictions made by samples.

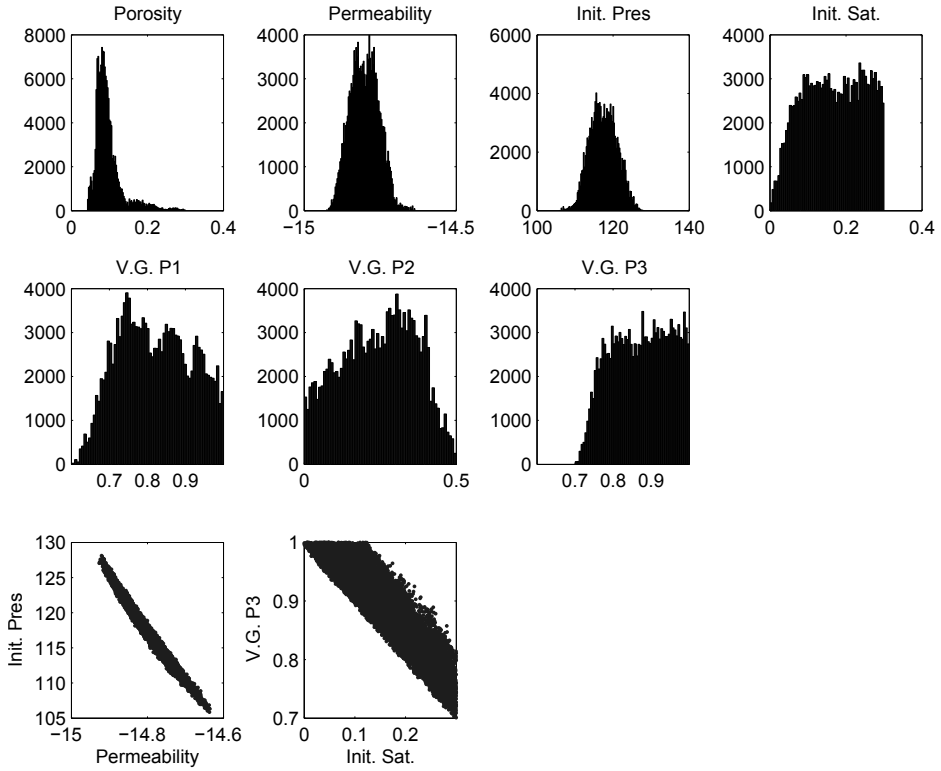

Figure 3: Histograms of the marginal distributions and scatter plots between parameters, synthesis data set.

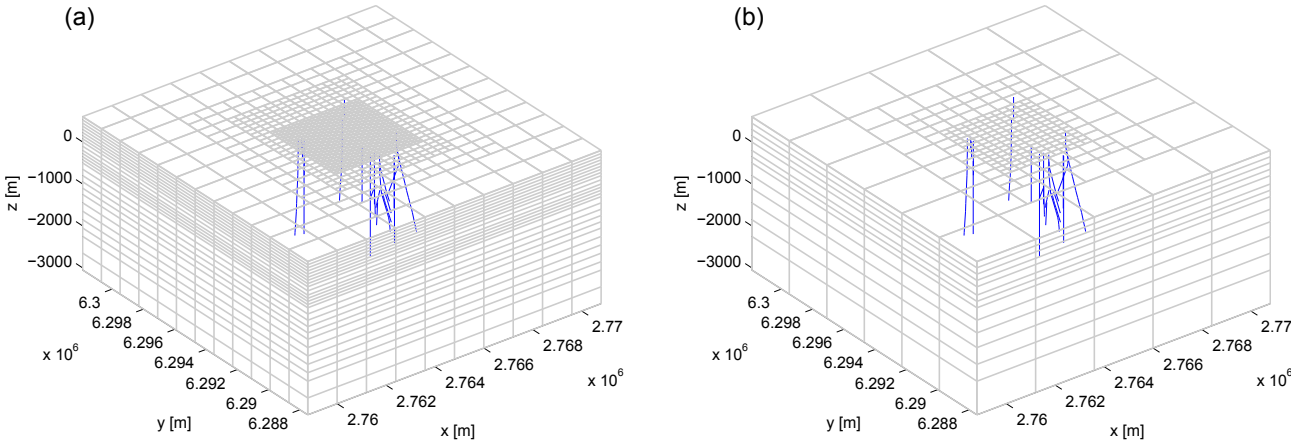

Figure 4: The fine grid (left) and the coarse grid (right) used for natural state modelling.

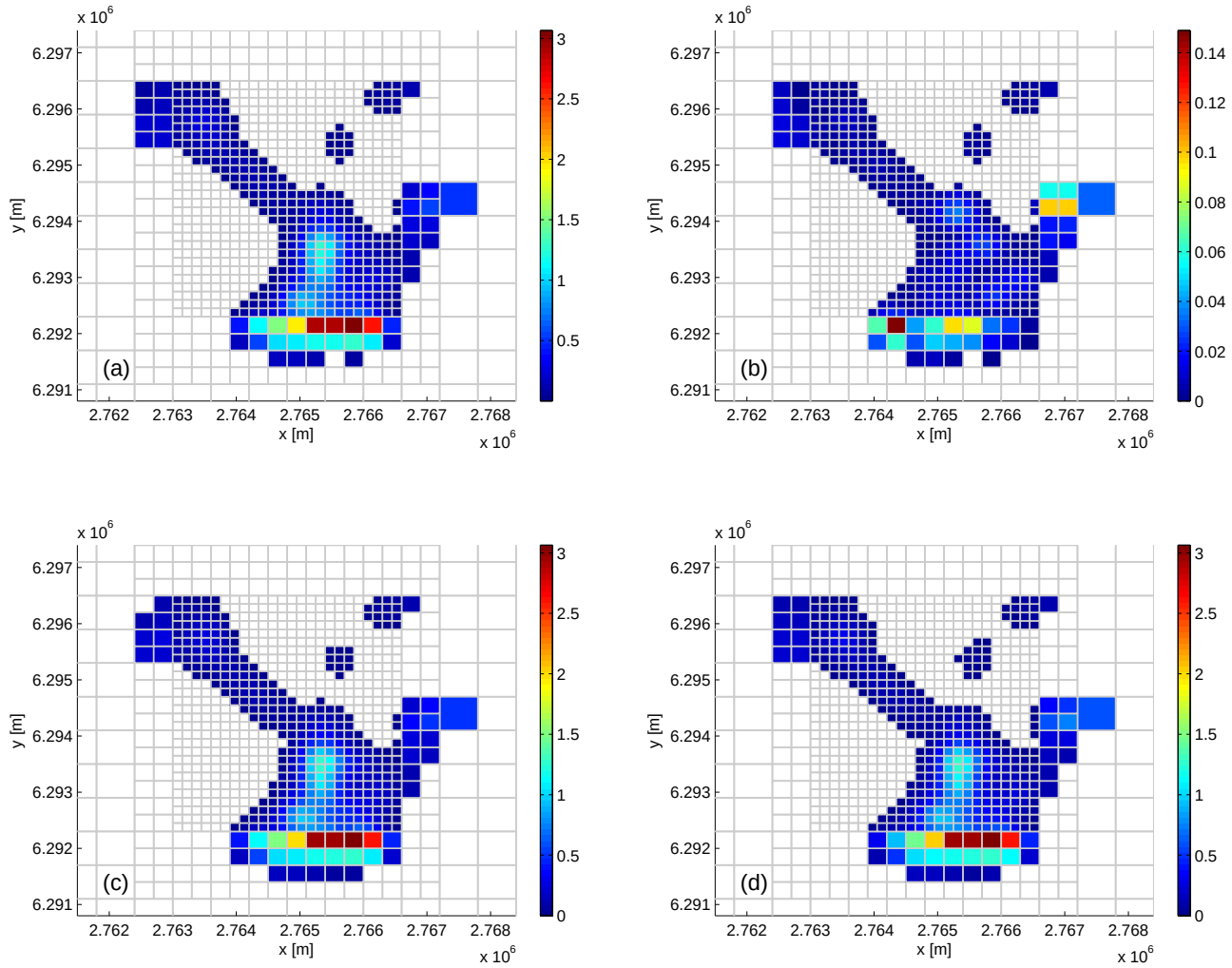

Figure 5: Distributions of mass input at the bottom of the model, unit in kg/s. (a): the mean realizations, (b): standard deviations of realizations, (c): one realization from the Markov chain, and (d): another realization from the Markov chain.

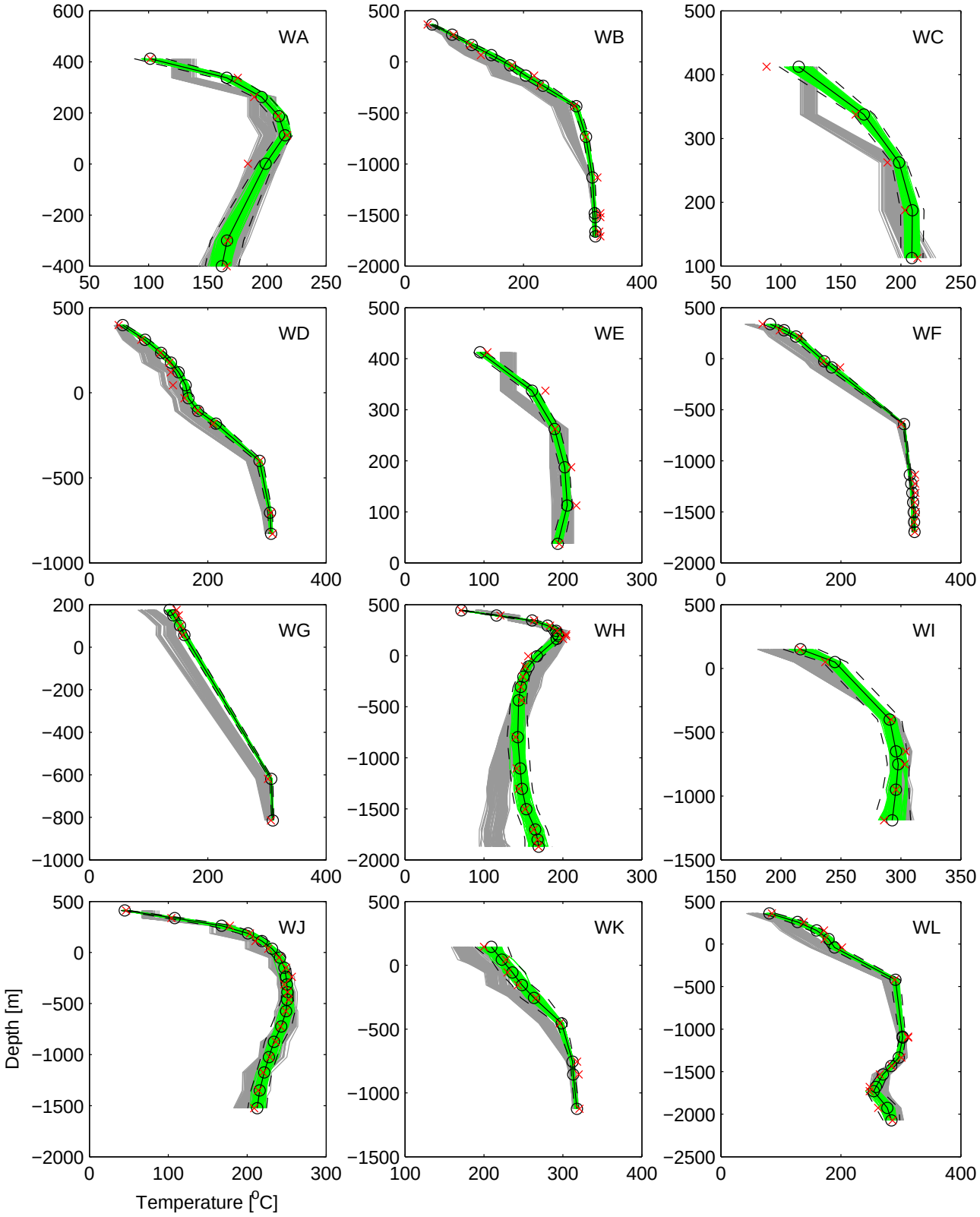

Figure 6: Comparison of estimated temperatures and measured data. The solid black lines are the estimated mean temperatures, dashed black lines are the 95% percent credible interval, and measured data are shown as red crosses. The green and gray lines represent outputs of the foaward model and the coarse model various realizations, respectively.

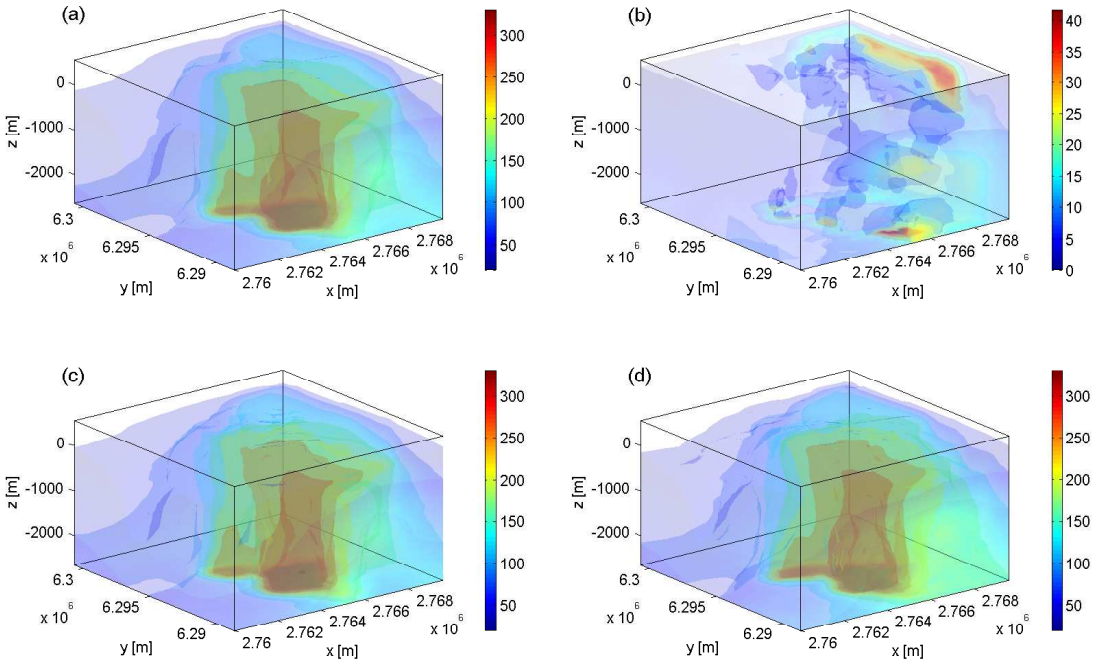

Figure 7: Distributions of model temperatures, unit is °C. (a): the mean realizations, (b): standard deviations of realizations, (c): one realization from the Markov chain, and (d): another realization from the Markov chain.

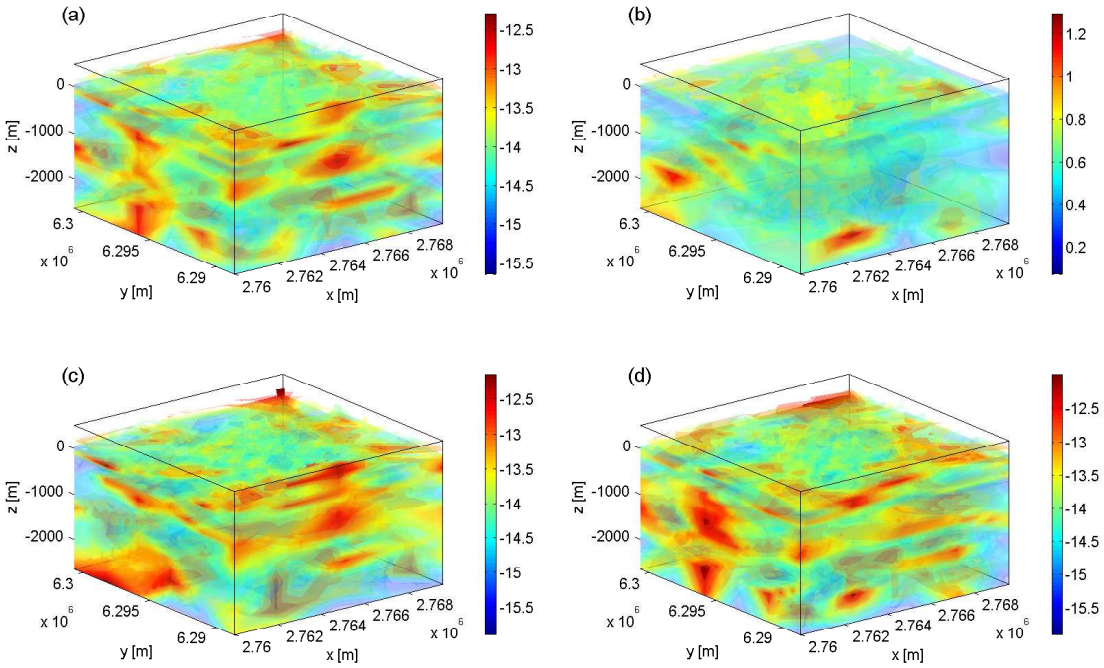

Figure 8: The permeability distribution on x direction, in base 10 logarithmic scale. (a): the mean realizations, (b): standard deviations of realizations, (c): one realization from the Markov chain, and (d): another realization from the Markov chain.

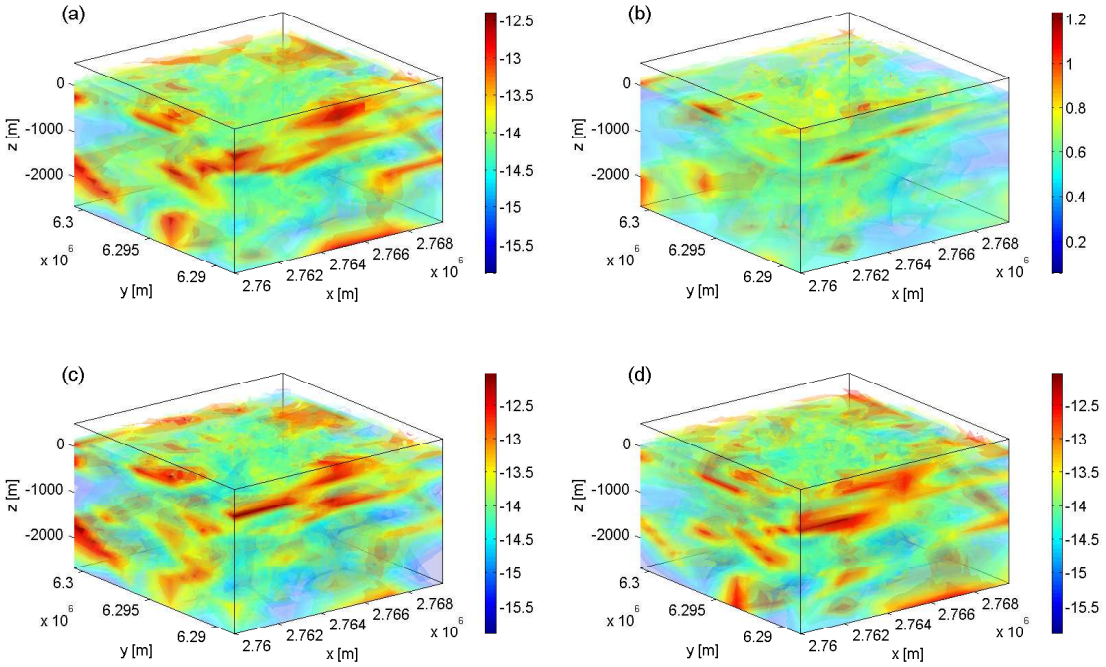

Figure 9: The permeability distribution on y direction, in base 10 logarithmic scale. (a): the mean realizations, (b): standard deviations of realizations, (c): one realization from the Markov chain, and (d): another realization from the Markov chain.

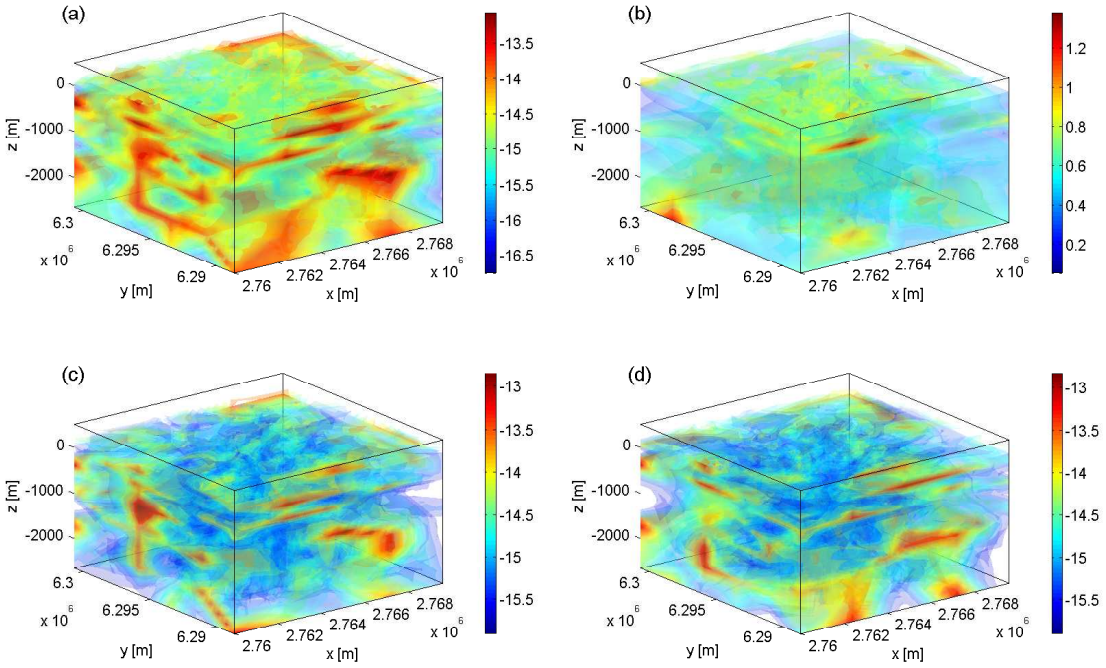

Figure 10: The permeability distribution on z direction, in base 10 logarithmic scale. (a): the mean realizations, (b): standard deviations of realizations, (c): one realization from the Markov chain, and (d): another realization from the Markov chain.